Band gap transmission in periodic bistable mechanical systems

Michael J. Frazier, Dennis M. Kochmann*

Graduate Aerospace Laboratories, California Institute of Technology, Pasadena, CA 91125, USA

ARTICLE INFO

ABSTRACT

We theoretically and numerically investigate the supratransmission phenomenon in discrete, nonlinear systems containing bistable elements. While linear waves cannot propagate within the band gaps of periodic structures, supratransmission allows large-amplitude waves to transmit energy through the band gap. For systems lacking bistability, the threshold amplitude for such energy transmission at a given frequency in the linear band gap is fixed. We show that the topological transitions due to bistability provide an avenue for switching the threshold amplitude between two well-separated values. Moreover, this versatility is achieved while leaving the linear dispersion properties of the system essentially unchanged. Interestingly, the behavior changes when an elastic chain is coupled to bistable resonators (in an extension of the well-studied linear locally resonant metamaterials). Here, we show that a fraction of the injected energy is confined near the boundary due to the resonators, providing a means of regulating the otherwise unrestrained energy flow due to supratransmission. Together, the results illustrate new means of controlling nonlinear wave propagation and energy transport in systems having multistable elements.

© 2016 Elsevier Ltd. All rights reserved.

1. Introduction

Phononic materials emerge from the periodic arrangement of small-scale building blocks which, through scattering and resonance phenomena, act to control the propagation of acoustic/elastic waves. This ability is demonstrated by the appearance of band gaps in the frequency spectrum. Outside of these gaps, the phononic material is transparent to vibrational waves, which propagate at different speeds dependent upon frequency and direction. Conversely, within the gaps, the material microstructure scatters and/or absorbs the wave energy, prohibiting transmission into the material in all or specific directions. Through careful design of the microstructure (where "microstructure" refers to the small-scale configuration as opposed to the macroscopic scale), the unique dynamics of phononic materials have been exploited at multiple length scales for a myriad of applications in engineering and physics (see, for example, [1,2] and the references therein). These results, based on a linear theory of wave propagation, pertain to waves of sufficiently small amplitude. Where wave amplitudes are large, the influence of nonlinear mechanisms within the material is apparent in the self-modulation of the wave field. Thus, in addition to microstructure design, wave control in phononic materials may feature an amplitude dependency. Moreover, the elicited nonlinear effects may counter the familiar behavior found in the linear regime.

---

* Corresponding author.
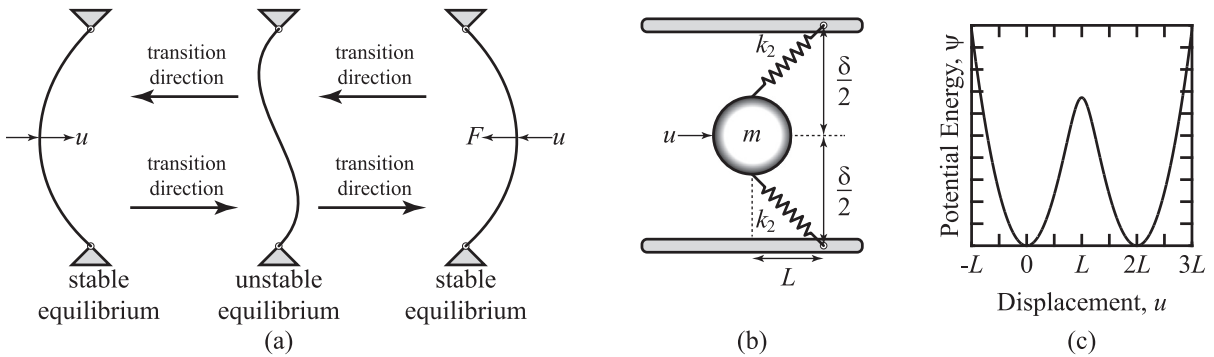   *E-mail address:* kochmann@caltech.edu (D.M. Kochmann).

Fig. 1. Mechanical bistability. (a) Buckled column transitioning between three equilibrium states under the influence of a centrally applied lateral load. (b) Mass–spring system as mechanical analog of buckled column. (c) Representative potential energy function $\psi(u)$ shows two local minima (stable equilibria) separated by a local maximum (unstable equilibrium).

Nonlinear supratransmission [3] is the sudden transparency exhibited by discrete nonlinear media subject to continuous boundary driving at a frequency within the linear band gap. Below a critical amplitude, the energy injected into such a system by the driven boundary spatially attenuates away from the driving due to wave reflection and is ultimately removed from the system by the driving. Above this amplitude threshold, the linear evanescent profile is unstable, resulting in the generation of mobile nonlinear modes (breathers, solitons, etc.) [4], i.e., energy transmission within the band gap.

The effect has been observed in a variety of integrable and non-integrable discrete systems, suggesting that it is a generic property of discrete nonlinear networks. While Geniet and Leon [3] introduced the phenomenon in the context of one-dimensional, homogeneous sine-Gordon and Klein–Gordon chains of coupled oscillators, theoretical and numerical work by themselves and others has extended to demonstrations in two-dimensional systems [5,6] and predictions of the threshold amplitude for Bragg [7] and multicomponent media [8]. For non-integrable systems, particularly those externally driven at a frequency outside the continuum limit, the Nonlinear Response Manifold (NLRM) method is a means for determining the critical magnitude of the forcing for supratransmission [9,10]. Utilizing NLRM and simulations, Maniadis et al. [11] predicted multiple forcing magnitude thresholds and Yousefzadeh and Phani [12] showed that, in the practical setting of finite structures, damping may eliminate the supratransmission phenomenon. By inserting an impurity into a discrete, nonlinear chain, Yu et al. [13] were able to control the emission rate of gap solitons and found damping imposed at the impurity improved the profile of the emitted waves. An alternative means of generating the effect which utilizes wave collisions has also been proposed [14]. Nevertheless, in the previous studies, *multistability*, a feature of some nonlinear systems, was either not permitted by the potential energy function or not investigated in detail by the authors. This represents a gap in the literature involving an entire category of nonlinear response. This also forgoes the flexibility of altering the system dynamic performance post-fabrication as demonstrated by Bernard and co-workers for linear waves in a one-dimensional system of locally bistable oscillators [15,16]. As a point of clarity, some works reference nonlinear *bistability* in the context of supra-transmission [17,5], however, these articles describe a range of driving amplitudes for which supratransmission and, its counterpart, infratransmission coexist. In this article, rather than describing the coexistence of two dissimilar transmission regions, bistability characterizes a network with two equilibrium configurations.

Multistability (i.e., the possession of two or more stable equilibrium configurations) is a property of a variety of physical [18–21], optical [22], chemical [23–25], and biological systems [26]. In mechanics, a classic example of a bistable system is provided by the buckled column (Fig. 1a). In response to a small lateral load, the column is displaced from its initial equilibrium configuration. With increasing load, the displacement grows until, at a critical value, the system snaps through to a second equilibrium configuration. During the transition between states, such bi- and multistable elements temporarily exhibit negative (static) stiffness, which, when constrained by the environment, can produce composites with effective damping [27,28] and (dynamic) stiffness [29] measures well beyond those of the constituent phases. A chain-like system for energy harvesting from sea waves [30] and recoverable, energy-absorbing cellular media [31] are but a few proposals utilizing bistable elements. In this article, we investigate bistability and the supratransmission phenomenon using a net-work of mechanically bistable elements previously shown to possess three amplitude-dependent propagation regimes [32].

Among phononic materials, metamaterials [33,34] are distinguished by their extreme/counterintuitive dynamic effective properties [35–39], the macroscale manifestation of subwavelength resonances. Moreover, where conventional phononic materials primarily utilize wave reflection to open spectral gaps, metamaterials exploit an additional wave absorption effect through the use of local resonators. To date, supratransmission has been studied in networks where wave reflection is the band-gap formation mechanism. It remains an open question how supratransmission, which permits energy propagation in the band gap, manifests in systems with an energy absorption capability and what impact resonator bistability (or lack thereof) imparts. Addressing these questions is an additional focus of this article for which we employ a second chain of oscillators with internal, bistable resonators.

The systems considered in much of the supratransmission literature model the behavior of optical waveguide arrays and

electrical transmission lines. Systems exhibiting this phenomenon raise opportunities for signal amplification [17] and transfer [6,40]. Similarly, one of the systems which we consider here finds application in mechanical logic gates [45]. However, the fundamental requirements for supratransmission being the possession of nonlinearity and band gaps, one can conceive of applications in a variety of periodic systems whose members experience a bistable energy potential, e.g., phase transitions, ferroelectric switching, physiological systems, etc. The conceptual lessons learned lay the foundation for the creation and analysis of mechanical systems whose linear and nonlinear response to incoming waves can be tuned in-dependently, which is of significant interest to applications ranging from sound insulation and acoustic cloaking to impact mitigation and vibration absorption.

The article is organized as follows: in Section 2 we present a discrete mechanical system whose on-site potential energy function is symmetric and possesses two local minima. We determine the band-gap frequencies from the linearized equations of motion, and give details on the simulation and the calculation of the transmitted energy. In Section 3, we discuss the results of simulation showing the presence of a single instance of nonlinear supratransmission in the medium of interest. We continue with a system possessing an asymmetric on-site potential, maintaining a single dispersive identity while permitting two, switchable supratransmission responses. Nonlinear monostable and bistable elements are locally attached to linear chains in Section 4 where we see the energy absorbing properties of internal resonators in the linear regime remain, in part, in a state of supratransmission. Finally, we close the article in Section 5 with concluding remarks and proposed directions.

2. Theory

2.1. Model description

In our study, the bistability of the buckled column is represented by the mass–spring system illustrated in Fig. 1b, consisting of a point mass m connected to two identical diagonal springs k_2 symmetrically arranged about the horizontal axis. Previously, this model was shown analytically and demonstrated numerically to possess three regimes of wave pro-pagation depending on the excitation amplitude [32]. Due to symmetry, a horizontal force applied to m will result in a horizontal displacement u, so we may treat the system as one-dimensional in the following. The total potential energy stored by the structure is given by

$$\psi(u) = k_2[\ell(u) - \ell(0)]^2 \tag{1}$$

where

$$\ell(u) = \sqrt{(L - u)^2 + (\delta/2)^2} \tag{2}$$

is the deformation of the springs as a function of the displacement. Fig. 1c, which plots Eq. (1) for arbitrary material and geometric parameters (obviously L, $\delta > 0$), reflects the bistability of the structure with two well-defined, local minima (i.e., equilibrium points) at $u = 0$, $2L$. In addition, the energy landscape is symmetric about $u=L$. From this unstable equilibrium position, the slightest perturbation causes the system in Fig. 1b to snap through to one of two stable configurations.

To study the effect of bistability on the supratransmission phenomenon, we take the system in Fig. 1b and construct a network of bistable elements connected by springs k_1 along the line of motion (Fig. 2). We use u^j to measure the horizontal displacement of the jth mass m. Consequently, accounting for the interaction potential, a network of N units has the La-grangian

$$\mathcal{L} = \sum_{j=1}^{N} \left[\frac{1}{2} m(\dot{u}^j)^2 - \psi(u^j) \right] - \sum_{j=1}^{N-1} \frac{1}{2} k_1(u^j - u^{j+1})^2 \tag{3}$$

from which the equations of motion can be written compactly as

$$\frac{d}{dt} \frac{\partial \mathcal{L}}{\partial \dot{u}^j} - \frac{\partial \mathcal{L}}{\partial u^j} = 0. \tag{4}$$

Or, explicitly,

$$m\ddot{u}^j + k_1(2u^j - u^{j+1} - u^{j-1}) + f(u^j) = 0 \tag{5}$$

where the force $f(u^j) = \psi'(u^j)$ applied to the jth mass m by the diagonal springs was introduced as

$$f(u^j) = -2k_2(L - u^j)\left[1 - \frac{\ell(0)}{\ell(u^j)}\right]. \tag{6}$$

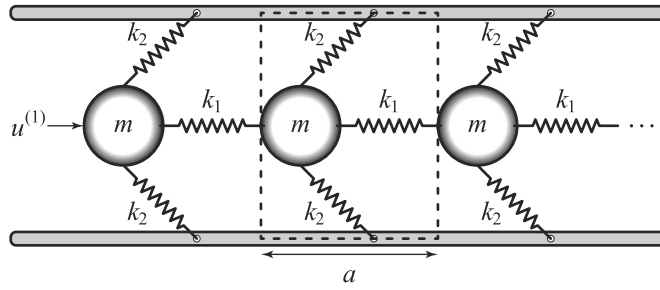Naturally, Eq. (6) is identically zero for u^j at the equilibrium positions.

Fig. 2. Periodic chain of bistable elements with lattice spacing a. The dashed box encloses the unit cell, the fundamental repeating structure of the chain.

2.2. Linear wave propagation

In isolating a single unit cell in Fig. 2, we can identify the forces F^j and F^{j+1} applied to the unit cell by its immediate neighbors to the left and right, respectively. In addition, we can relate those forces to the displacements u^j and u^{j+1} as follows:

$$\frac{m}{2}\ddot{u}^j + k_1(u^j - u^{j+1}) + f(u^j) = F^j, \tag{7a}$$

$$\frac{m}{2}\ddot{u}^{j+1} - k_1(u^j - u^{j+1}) = F^{j+1}, \tag{7b}$$

where the masses are halved so that the total mass of the unit cell remains m.

Now, we consider Bloch wave propagation through the phononic material, i.e., the propagation of plane waves through a chain of infinite extent. Consequently, Eqs. (7) are linearized about the stable equilibrium $u^j = u_0$ such that, for $|u^j| \ll L$, Eq. (6) is approximated by

$$f(u^j) = k_L u^j = 2k_2\left(1 - \frac{(\delta/2)^2\sqrt{L^2 + (\delta/2)^2}}{[(L - u_0)^2 + (\delta/2)^2]^{3/2}}\right)u^j, \tag{8}$$

where u^j is measured from u_0, and boundary displacements are related by the propagation constant γ according to

$$u^{j+1} = \gamma u^j, \quad \gamma = e^{i\kappa a} \tag{9}$$

with wavenumber κ. For a wave of amplitude U and radial frequency ω, the time-dependent displacement is $u^{j+n}(t) = U^{j+n}e^{\pm i\omega t}$, $n \in \mathbb{N}$. Together, Eqs. (7)–(9) are incorporated in matrix form as

$$\begin{bmatrix} -\dfrac{m}{2}\omega^2 + k_1 + k_L & -k_1 \\ -k_1 & -\dfrac{m}{2}\omega^2 + k_1 \end{bmatrix}\begin{bmatrix} 1 \\ \gamma \end{bmatrix}u^j = \begin{bmatrix} F^j \\ F^{j+1} \end{bmatrix}. \tag{10}$$

Thus, pre-multiplying Eq. (10) by $[1\ 1/\gamma]$ establishes an eigenvalue problem (cell equilibrium requires $F^j + F^{j+1}/\gamma = 0$) [41]. Following the determinant, we have the characteristic

$$\gamma^2 k_1 + \gamma(m\omega^2 - 2k_1) - 2k_2\gamma\left(1 - \frac{d^2\sqrt{1 + d^2}}{[(1 - \bar{u}_0)^2 + d^2]^{3/2}}\right) + k_1 = 0, \tag{11}$$

where $d = \delta/2L$ and the normalized displacement $\bar{u}^j = u^j/L$. For linear wave propagation, this is the dispersion relation. In the present case, with stable equilibria at $\bar{u}_0 = 0, 2$ (i.e., $u_0 = 0, 2L$), the initial stable configuration of the chain is inconsequential to the dynamic analysis to follow. In solving for γ, the real (propagating) and imaginary (attenuating) components of the normalized wavenumber $\kappa a = \kappa_R a + i\kappa_I a$ are extracted as follows:

$$\kappa_R a = |\operatorname{Re}[i \ln\gamma]|, \tag{12a}$$
$$\kappa_I a = |\operatorname{Im}[i \ln\gamma]|. \tag{12b}$$

Due to the discrete nature of the medium under investigation and the condition $\kappa_R a = -\kappa_R a$, independent propagating waves are confined to $\kappa_R a \in [0, \pi]$. In addition, a conservative system guarantees $\kappa_I a \neq 0$ if $\kappa_R a = 0$ or π [42]. In the following, we adopt the material and geometric parameters $m=1$, $k_1 = 10$, $k_2 = 1$, and $d = 1/5$, all of which are normalized by unit values.

As depicted in Fig. 3, in the linear regime, the system possesses two forbidden band gaps (shaded areas) – one defined for $\omega > 6.474$ and the other for $\omega < 1.386$. In the following, our study will focus on energy transmission via nonlinear modes within the lower gap.

2.3. Simulation and energy transmission

Energy transmission properties of the network are investigated utilizing a driven boundary. In our study, the driven boundary takes the form of a prescribed harmonic displacement $\bar{u}^{(1)}(t) = \bar{U} \sin \omega t$. Following [3], in order to mitigate the shock associated with an abrupt change from zero initial velocities, the initial oscillator velocities are chosen to fit an evanescent profile as determined by Eqs. (12) for the particular driving frequency at hand. Specifically,

$$\bar{u}^j(0) = 0 \quad \dot{\bar{u}}^j(0) = \omega \bar{U} \cos[(j-1)\kappa_R a] e^{-(j-1)\kappa_I a}. \tag{13}$$

Following the integration scheme in Ref. [43], simulations are performed for a duration of $\Delta t = 200T$, where T is the period of the driving. The simulation domain consists of a chain of 1000 cells with a linearly increasing viscous damping $c\dot{u}^j$ applied to the final $j \geq 500$ cells in order to minimize the reflection of phonons and envelop solitons and mimic an infinite medium. The response of the damped cells, however, is not considered in our study. Kink solitons are managed by extending the medium beyond 1000 units.

Over the simulation time, the energy injected into the medium by the driven boundary is given by

$$E_{in} = \int_0^{nT} k_1 [\bar{u}^{(2)} - \bar{u}^{(1)}] \dot{\bar{u}}^{(1)} dt \quad n \in \mathbb{N}. \tag{14}$$

In the linear case, E_{in} vanishes in the band gap over an integer multiple of the period due to wave reflection.

3. Supratransmission results

3.1. Symmetric local potential

To investigate nonlinear supratransmission in the network of bistable oscillators in Fig. 2, we set a constant driving frequency of $\omega = 1$ in the band gap and, between each simulation, vary the amplitude of the driving so as to bridge the two equilibrium configurations, i.e., $\bar{U} \in (0, 2]$. The initial configuration of the chain is such that $\bar{u}_0 = 0$, although, as mentioned in Section 2.2, $\bar{u}_0 = 2$ will yield similar results. Fig. 4 depicts simulation snapshots of the system response associated with different driving amplitudes after $\Delta t = 200.25T$ (the additional quarter period facilitates comparison with the evanescent profile). As expected, for small amplitudes, the sites nearest the driving have the greatest displacement consistent with a linear response; energy is concentrated at the boundary. For sufficiently large amplitudes, the evanescent response is unstable and energy is carried through the network (Figs. 4b and c). Notice, the significant difference in response between Figs. 4b and c is compared to the relatively small increase in driving amplitude. This difference is analyzed below. It should be noted that although the driving amplitude in Figs. 4b and c causes some sites near the boundary to enter the second energy well of Fig. 1b, they do not necessarily attain the second equilibrium configuration or remain there, and so the generation of topological (kink) solitons is avoided. Nevertheless, in the case that topological solitons are generated, the system is extended to prevent reflections.

Fig. 5a offers a more detailed illustration of the supratransmission phenomenon where the injected energy (14) is displayed as a function of the driving amplitude. The results shown for driving at $\omega = 1$ are typical and representative of excitation at other frequencies in the lower band gap. Similar to Ref. [11], which applied harmonic forcing of different magnitude (we apply harmonic displacement), there are three regimes of energy transmission. In the linear regime approximated by Region I, relatively little energy in the form of phonons is transmitted through the medium due to the efficiency of wave reflection. This is the response shown in Fig. 4a. However, as depicted in Fig. 4b, with increasing excitation amplitude, the network becomes more transparent. In Region II, weak wave propagation occurs (Fig. 4b). An inspection of the associated frequency content reveals that the waves belong primarily to harmonics of the driving that fall in the pass band of Fig. 3 and are the twinkling modes described, e.g., in Ref. [44]. This is supported by our investigations at different driving frequencies, where we notice that the onset of this transmission generally occurs in the vicinity of the driving amplitude at which first $\bar{u}^{(2)} > 1$. For the present scenario where $\omega = 1$, the driving amplitude for this first snapping event ($\bar{U} = 1.002$) is indicated in Fig. 5b, which shows the maximum number of sites simultaneously in the second energy well during the simulation. After the first snapping event, this number steadily increases but remains relatively low (less than 10) until $\bar{U} = \bar{U}_{th} = 1.65$, after which, the number of snapping sites dramatically increases. Coincidently, in Fig. 5a, the energy input experiences a sudden escalation. This is nonlinear supratransmission resulting from a breakdown in the linear wave solution, which is illustrated in advancing from Fig. 4b to c, and $\bar{U}_{th} = 1.65$ is the threshold amplitude.

This result for a bistable chain whose elements are uniformly in the same initial configuration represents the ideal scenario. In practice, the system may contain several elements arranged counter to the primary, intended configuration which may affect the value of the supratransmission threshold. Fig. 6 summarizes the results of an investigation on the impact of defects [i.e., one or a series of contiguous elements (a cluster) initially at $\bar{u}_0 = 2$ rather than the primary $\bar{u}_0 = 0$] in our bistable system. In particular, Fig. 6b emphasizes the importance of the interaction spring k_1 to the existence of irregularities within the chain. For different k_1, we initialize the system with all elements at $\bar{u}_0 = 0$ except the defect element(s), which are initialized at $\bar{u}_0 = 2$ and placed well within the chain (centered at $j = 250$). After $\Delta t = 200T$, we plot the fraction of

the original defect element(s) which remain defective. Below $k_I = 1/4$, the interaction between elements of the chain is so weak as to allow for a single defect element to survive. Above this value (e.g., the present case), the neighboring sites act to eliminate the irregularity. Fig. 6b further indicates that similar results proceed from several defects if they are isolated and dispersed within the chain; however, greater interaction stiffnesses are tolerable if the defect is a cluster. Naturally, being an unintended development, an irregularity may arise at any location within the system. Considering, separately, a single and clustered defect, Fig. 6c illustrates the diminishing impact of a defect on $\bar{U}_{th}$ as it is situated further within the chain and the threshold approaches $\bar{U}_{th} = 1.65$. Also indicated is the general decrease in $\bar{U}_{th}$ with increasing population of defect sites. For a given percentage of dispersed and randomly positioned defects, Fig. 6d reveals two trends: (1) the threshold amplitude generally decreases with increasing defect population and (2) the threshold value becomes less certain with greater defect percentages – a combined effect of defect density and position. Ten simulations were run at each defect percentage.

3.2. Asymmetric local potential

In the preceding section, we examined the phenomenon of nonlinear supratransmission in a network of bistable oscillators; however, the uniqueness of bistability was not made apparent due to the symmetry of the local potential. As a
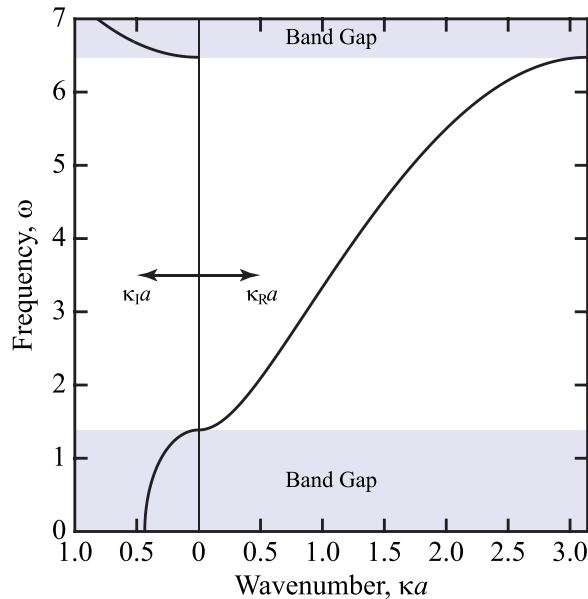

Fig. 3. Frequency band diagram. Waves with frequency in the pass band (unshaded region) penetrate the medium. In the band gaps (shaded regions), waves attenuate over space and do not propagate into the material.
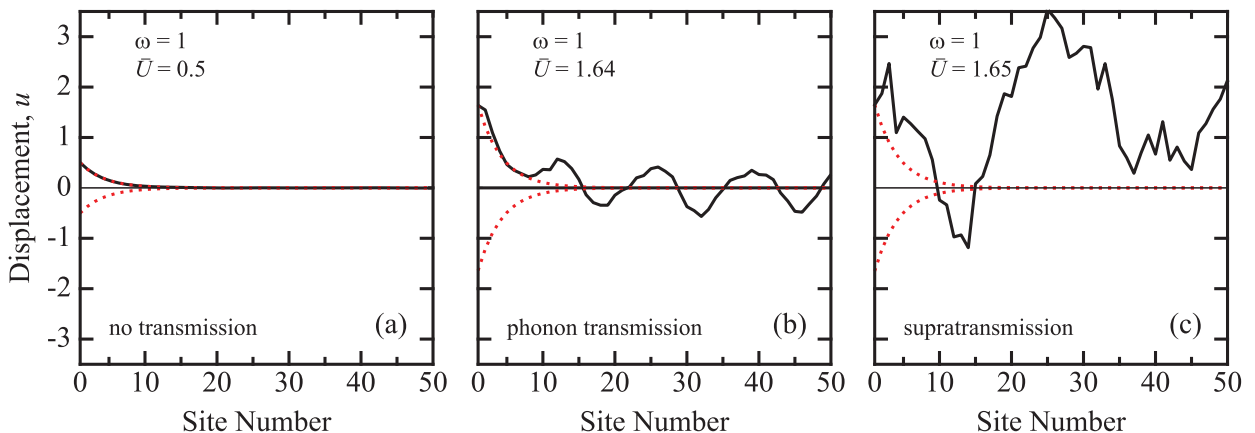

Fig. 4. (color online) Snapshots of chain displacement profile (black curve) at $\Delta t = 200.25T$ for the first 50 sites with driving amplitudes resulting in (a) no energy transmission, (b) weak phonon transmission, and (c) strong nonlinear transmission (supratransmission). The red, dashed curve marks the limits of a linear (evanescent) response.
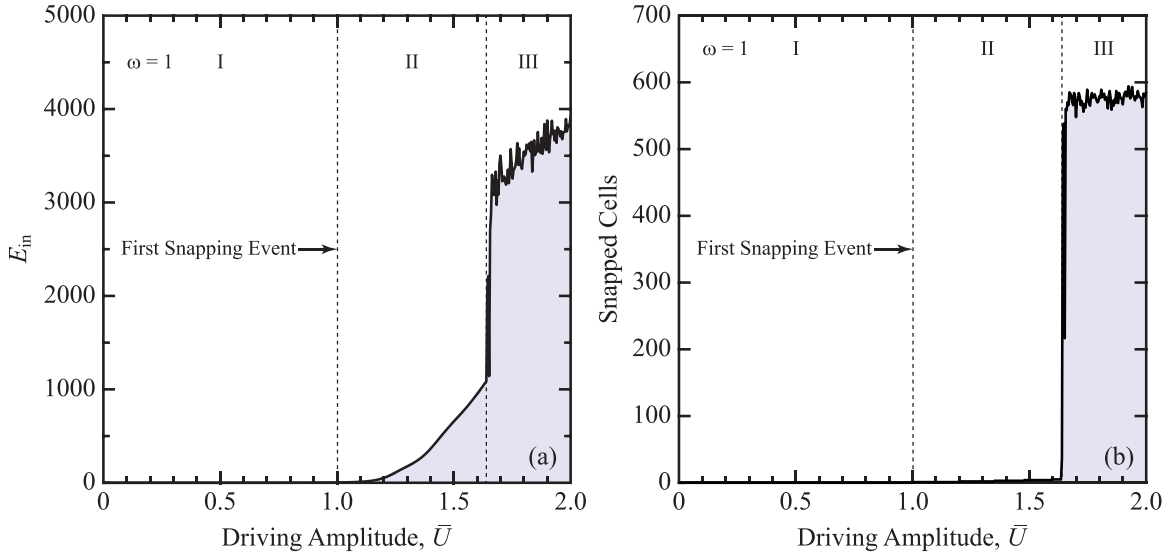
Fig. 5. Supratransmission from symmetric local potential. (a) Energy transmission as a function of driving amplitude. (b) Number of cells in the region $j \in [2, 500]$ that snapped during the simulation.

consequence of the symmetry, the dynamics of energy transmission are identical regardless from which of the two configurations the chain of oscillators is analyzed. This motivates an investigation of supratransmission in a network of oscillators with an asymmetric local potential where the nonlinear environment depends on the initial configuration of the system. To break the symmetry, the quadratic potential $\psi_0 = k_3(u - 2L)^2/2$ is added to Eq. (1), which elevates one energy well over the other as the energy of this stable equilibrium ψ_1 approaches that of the unstable equilibrium ψ_s (Fig. 7b). This physically represents the insertion of a local horizontal spring k_3 as in Fig. 7a which is relaxed at $u = 2L$.

To reveal the impact of this new asymmetric, bistable on-site potential on energy transmission requires a reformulation of the equations of motion to account for the additional spring k_3. Thus, Eq. (6) is rewritten as

$$f(u^j) = -2k_2(L - u^j)\left[1 - \frac{\ell(0)}{\ell(u^j)}\right] + k_3(u^j - 2L).$$

(15)

Following the same procedure described in Section 2.2 above, the dispersion relation is

$$\gamma^2 k_1 - \gamma(2k_1 + 2k_2 + k_3 - m\omega^2) + \gamma\frac{2d^2 k_2 \sqrt{1 + d^2}}{[(1 - \bar{u}_0)^2 + d^2]^{3/2}} + k_1 = 0$$

(16)

with $d = \delta/2L$.

Keeping the same material and geometric parameters as before and setting $k_3 > 0$, Fig. 7b plots one possible asymmetric on-site potential. There is one stable equilibrium configuration ($\bar{u}_0 \neq 0$) where together k_2 and k_3 store some deformation energy $\psi_1 \neq 0$, and a second ($\bar{u}_0 = 2$) where no energy is stored ($\psi_2 = 0$). In transitioning from one configuration to the next, the system passes through an unstable equilibrium with energy $\psi_s > \psi_1$. While the bistable on-site potential nonetheless presented a single wave-propagation environment in the previous chain design, in this asymmetric case, it offers two opportunities for supratransmission. However, as supratransmission results from the instability of the linear solution, in order to adequately compare energy transmission from each arrangement, we must have each configuration be dynamically equivalent from the perspective of linear waves. In practice, if circumstances require, this condition may be lifted. Already, Bernard and co-workers have shown theoretically [15] and demonstrated experimentally [16] the reconfiguration of the band structure in a 1D system with on-site bistability. However, the topic of supratransmission was not addressed.

Setting $k_3 = 1/5$, Fig. 7c depicts the frequency band diagram associated with linear wave propagation within each energy well. Excellent agreement is seen between the two curves, indicating that the linear waves observe essentially the same material regardless of the chain configuration. In fact, despite $\psi_1/\psi_s = 0.47$, for $\omega = 1$, the imaginary wavenumbers are in good agreement, i.e., $|\kappa_I^{(1)} - \kappa_I^{(2)}|a < 0.01$ where the superscripts refer to the first and second system configurations. Nevertheless, Fig. 8a draws a different picture for nonlinear supratransmission. Excitation from the first network configuration, where the springs k_2 and k_3 are initially deformed, results in enhanced energy transmission at a smaller driving amplitude than if the excitation initiates in the second system configuration. In addition, prior to supratransmission, the energy injected into the network by the driven boundary is less in the first case compared to the second. Each of these effects is a consequence of the asymmetry in the local potential: the energy well corresponding to the first configuration possesses a smaller mouth, requiring a smaller driving amplitude, and is shallower, requiring less energy input. Fig. 8b shows the separation and migration of the threshold amplitudes over a range of k_3. Bistability (in general, multistability) is a mechanism for switching
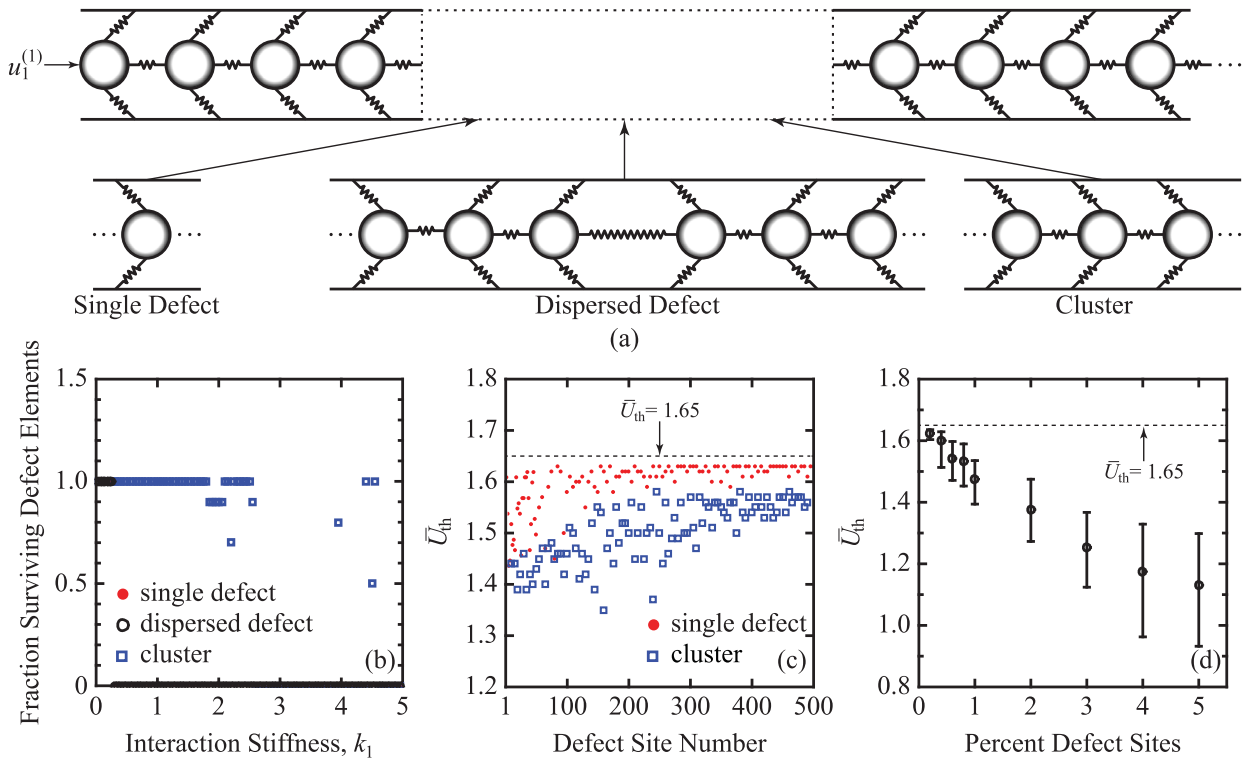
Fig. 6. (color online) Defects in bistable chain. (a) Uniform chain with single, dispersed, and cluster defects. (b) Fraction of defect element(s) which survive after $\Delta t = 200T$. (c) Supratransmission threshold amplitude as a function of defect location. (d) Shift in the mean (open circles) and range (bars) of the supratransmission threshold gathered from ten simulations with a percentage of randomly located defect sites.

among alternate material properties. Here, we have presented a discrete material that possesses one response to small-amplitude excitation, but, due to bistability, two different responses when the excitation becomes large. This is one of our principal results.

4. Energy distribution in chains with bistable local resonators

To date, insight into the supratransmission phenomenon has been garnered from a variety of systems of a theoretical and practical nature. However, to the best of our knowledge, studies have only considered networks where the band gap is generated by wave reflection. Energy absorption by local resonating units, exploited in many optical and acoustic/elastic metamaterial designs, is another mechanism of band-gap formation and represents an unexplored avenue in the study of supratransmission. This motivates the questions: Is supratransmission energy flow curtailed in systems with an energy absorption capability? In systems with bistable resonators? To answer these questions, we use the unit cell depicted in Fig. 9a to investigate two networks of oscillators. In particular, the unit cell constructs a linear chain with attached nonlinear resonators, embedding an oscillator of the type described in Section 3.2 within a linear chain. Depending on the stiffness k_3 (assuming k_2, L, and δ are fixed), the response of the internal resonator may be simply nonlinear or possess the additional feature of bistability.

The material properties are chosen to be consistent with many metamaterial realizations, in particular Ref. [33]. We set $m_1 = 1$, $m_2 = 10$, $k_1 = 10$, and $k_2 = 1$. With the geometry newly defined by $d = \delta/2L = 1$, the system is bistable for any $k_3 < 0.18$. For the simulation, we chose $k_3 = 1/5$ to describe a resonating system with only a single stable configuration and, for simplicity, set $k_3 = 0$ for a chain with bistable internal resonators. As above, now for a two-component cell, for small-amplitude waves, we linearize the equations of motion and apply the Bloch boundary conditions [41] to formulate the dispersion relations. In each case, a dispersion analysis reveals a resonance gap in the continuum limit which includes the driving frequency $\omega = 0.5$ (see Fig. 9b).

In executing the simulations, our interest is in the distribution of energy in the chain following the onset of supra-transmission. In systems without local resonators, away from the driving boundary, lattice sites observe the same total energy on average over time. To determine if this is the case for the two present systems, we calculate the total on-site energy at each time-step during the simulation according to
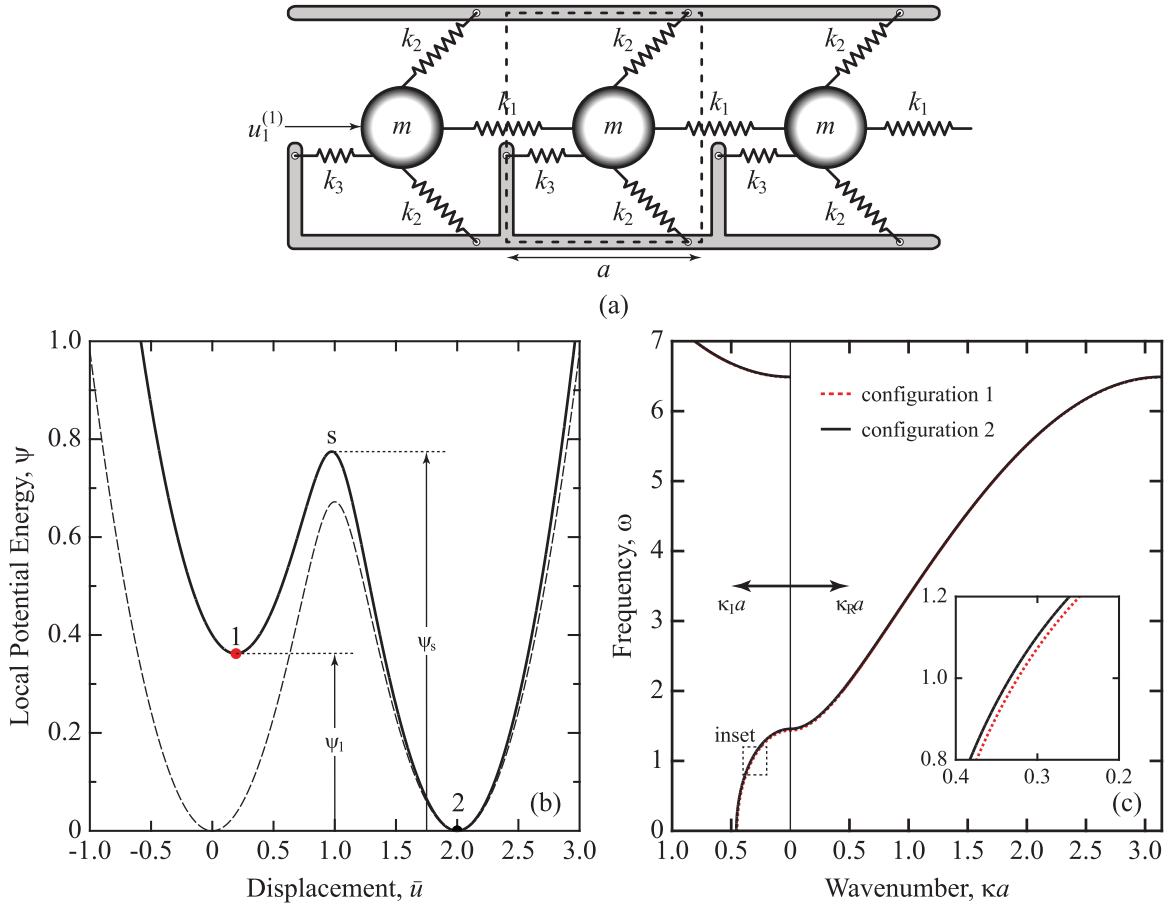
Fig. 7. (color online) (a) Original system (Fig. 2) with an additional horizontal spring k_3 acting locally. Although depicted separate from k_1 for clarity, k_3 acts along the line of motion. (b) On-site potential energy adjusted by ψ_0. The labels "1" and "2" indicate the first and second equilibrium positions, respectively; the label "s" is the unstable "snap-through" position. The stored energy at positions "1" and "s" are, respectively, ψ_1 and ψ_s. The dashed curve is the original potential function ($k_3 = 0$). (c) Frequency band diagram for linear waves in the first (red, dashed) and second (black) energy well. The inset details the lower band gap and the slight discrepancy between the results of each energy well.
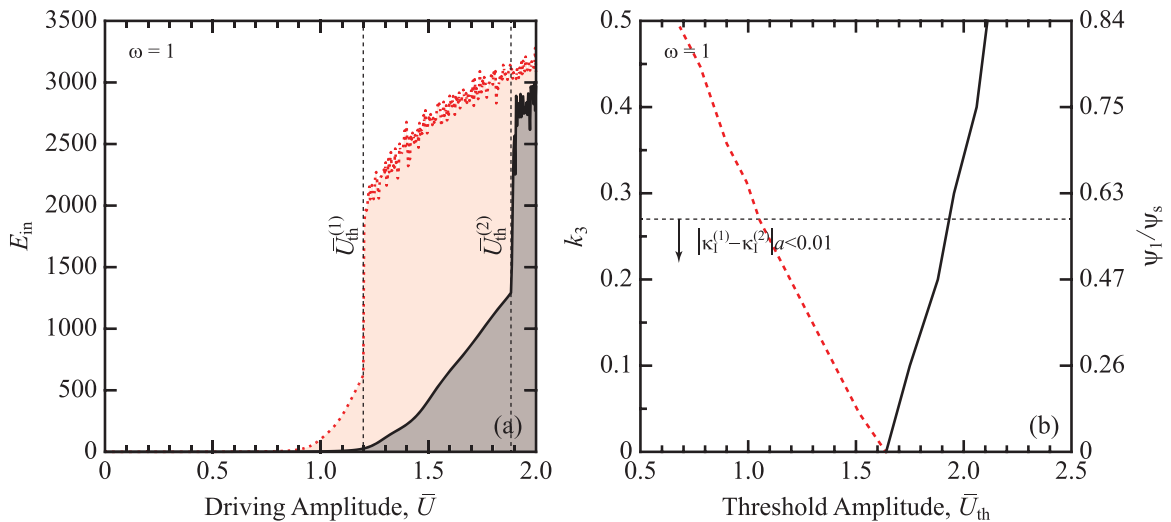

Fig. 8. (color online) (a) Supratransmission from asymmetric local potential with either the first (red, dashed) or second (black) configuration as the reference. (b) The migration of the threshold amplitudes $\bar{U}_{th}$ ["1" (red, dashed) and "2" (black)] with increasing stiffness k_3. For stiffness below the dashed line, the wavenumbers of each reference configuration agree to the third decimal.
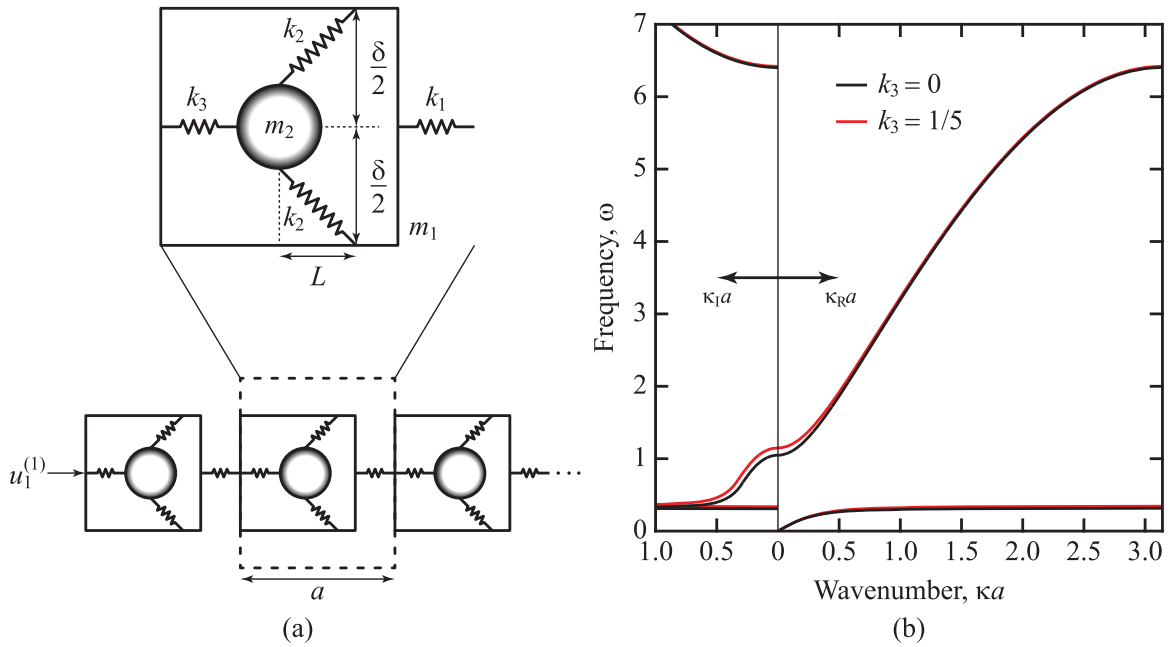
Fig. 9. (color online) (a) Chain of oscillators with linear coupling and internal, bistable resonators. Essentially, the bistable oscillator described in Section 3.2 is embedded within a linear chain. (b) Frequency band diagram corresponding to linear wave propagation within the chain of oscillators with nonlinear resonators. The spring k_3 tunes the resonator stability between the alternatives: bistable (black) with stiffness $k_3 = 0$ and monostable (red, dashed) with stiffness $k_3 = 1/5$. Wave energy is reflected in the upper band gap; it is absorbed in the lower band gap by the resonators.
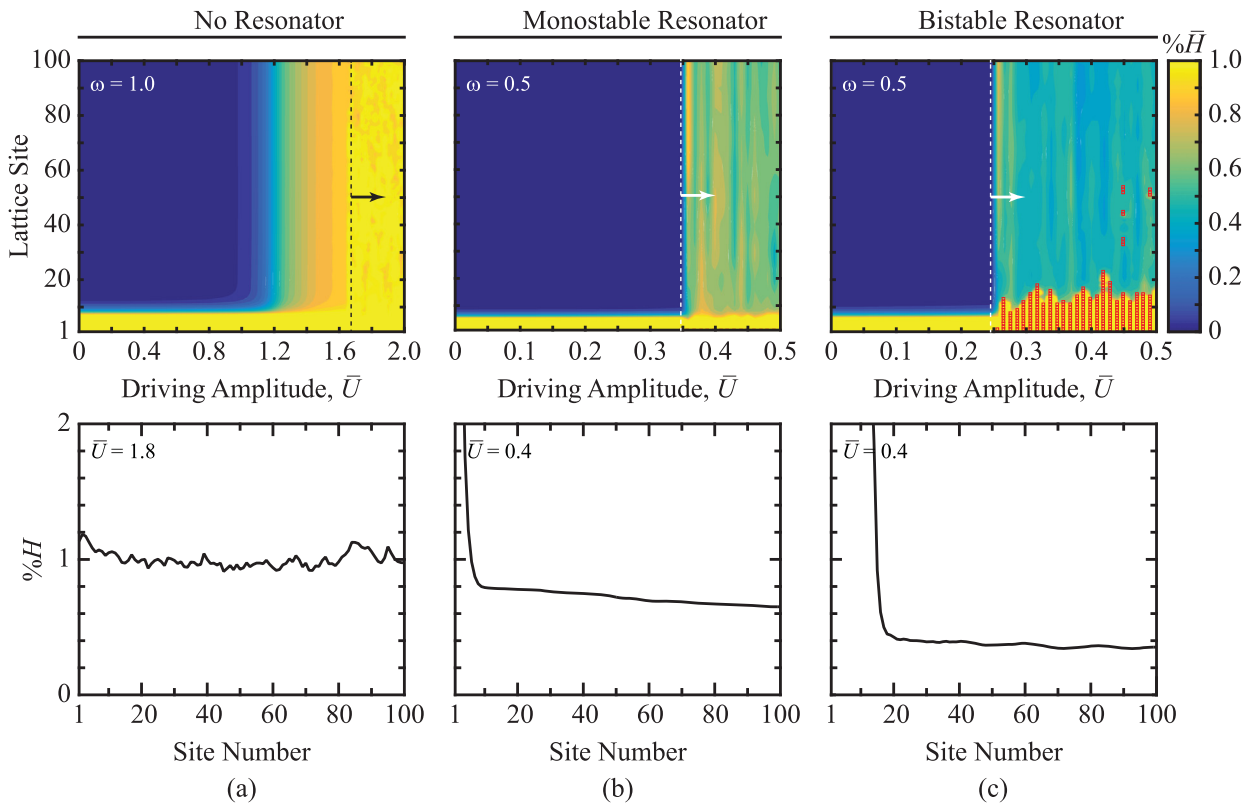

Fig. 10. (color online) Total on-site energy distribution. The percentage of the time-averaged total on-site energy in the first 100 sites of (a) the non-resonant system of Section 2.1, (b) a linear chain with local nonlinear, monostable resonators, and (c) a linear chain with internal bistable resonators. In the top row, the dotted line and arrow indicate the region of supratransmission in each system. Square markers (red) identify the lattice sites where u_2 entered the second energy well. The bottom row details the energy distribution for a particular driving amplitude in the supratransmission region. (a) Energy is evenly distributed among all sites during supratransmission. (b, c) Energy is localized near the boundary during supratransmission, decreases rapidly and non-exponentially over the first few sites, and then, is evenly distributed among the remaining sites.

$$\mathcal{H}^j = \tfrac{1}{2}\Big[m_1(\dot{\bar{u}}_1^j)^2 + m_2(\dot{\bar{u}}_2^j)^2 \Big] + \tfrac{1}{2}k_1(\bar{u}_1^j - \bar{u}_1^{j+1})^2 + \psi(\bar{u}_1^j, \bar{u}_2^j),$$

(17)

where

$$\psi(\bar{u}_1^j, \bar{u}_2^j) = k_2\Big[\sqrt{(1 + \bar{u}_1^j - \bar{u}_2^j)^2 + d^2} - \sqrt{1 + d^2} \Big]^2.$$

(18)

Integrating over time,

$$\bar{\mathcal{H}}^j = \int_{t_1}^{nT} \mathcal{H}^j \mathrm{d}t$$

(19)

we choose $t_1 \neq 0$ to ensure sufficient time for wave energy to propagate to all undamped sites. For the present set of simulations, we restrict this to the first 100 undamped sites, well into the chain. To compare between different driving amplitudes, Eq. (19) is normalized by the sum $\sum_{j=1}^{100} \bar{\mathcal{H}}^j$ for the particular driving amplitude.

Fig. 10 shows the results for three networks under consideration: one without attached resonators and two with internal nonlinear, monostable and bistable resonators, respectively. The first row plots Eq. (19) (normalized as previously described) over a range of driving amplitudes. The non-resonant example is taken from Section 3.1. Prior to supratransmission, Fig. 10a shows that wave energy is localized near the driving boundary, gradually decaying further into the medium. During supratransmission, however, the injected energy is nearly evenly distributed among the lattice sites as energy flows essentially unconstrained from the boundary into the medium. The second row of Fig. 10, showing $\bar{\mathcal{H}}^j$ for a specific driving amplitude, more clearly illustrates this point. We also observed this in chains modeled by the discrete sine-Gordon equation (not shown). Focusing on the monostable system in Fig. 10b shows that, during supratransmission, only some wave energy radiates into the medium; much of the energy remains close to the boundary, largely absorbed by the resonating units in the first few lattice sites. Turning to the chain with bistable resonators, in Fig. 10b, we see a similar effect; much of the energy remains close to the boundary. In each of these two cases, further inspection of the spectral content of shows that the response is nonlinear near the driving boundary, but linear (composed of higher harmonics) in the later sites. Both Figs. 10b and c suggest that internal resonators may act to regulate the amount of energy flow during supratransmission.

5. Conclusions

In summary, we investigated the supratransmission phenomenon in one-dimensional chains characterized by bistability, a feature not explored in previous studies. We highlighted the ability of bistable systems to exhibit two amplitude thresholds beyond which harmonic driving in the band gap will propagate energy. The effect stems from an asymmetric on-site potential and allows supratransmission applications greater flexibility. Nevertheless, a network with the appropriate material and geometric parameters may still display a unique dispersive response. Counter to the conventional reflective systems, we also examined two cases of absorptive mediums as linear chains with internal resonators that were either simply nonlinear or bistable. While wave energy is evenly distributed throughout a non-resonant system under supratransmission, it is localized near the boundary for resonant cases. However, energy does not attenuate exponentially within the network; instead, there is a sharp separation between supratransmission at the boundary (where energy is concentrated) and linear transmission in the remaining sites. This demonstrates the capacity of resonant systems to regulate the flow of supratransmission energy. Together, the results illustrate different forms of control over the phenomenon in support of applications.

References

[1] M.I. Hussein, M.J. Leamy, M. Ruzzene, Dynamics of phononic materials and structures: *historical origins, recent progress, and future outlook*, *Appl. Mech. Rev.* 66 (May) (2014) 040802.
[2] M. Maldovan, Sound and heat revolutions in phononics, *Nature* 503 (November) (2013) 209–217.
[3] F. Geniet, J. Leon, Energy transmission in the forbidden band gap of a nonlinear chain, *Phys. Rev. Lett.* 89 (September) (2002) 134102.
[4] J. Leon, Nonlinear supratransmission as a fundamental instability, *Phys. Lett. A* 319 (December) (2003) 130–136.
[5] J.E. Macías-Díaz, Numerical study of the transmission of energy in discrete arrays of sine-Gordon equations in two space dimensions, *Phys. Rev. E* 77 (January) (2008) 016602.
[6] J.E. Macías-Díaz, Bistability of a two-dimensional Klein–Gordon system as a reliable means to transmit monochromatic waves: *a numerical approach*, *Phys. Rev. E* 78 (November) (2008) 056603.
[7] J. Leon, A. Spire, Gap soliton formation by nonlinear supratransmission in Bragg media, *Phys. Lett. A* 327 (July) (2004) 474–480.
[8] P. Anghel-Vasilescu, J. Dorignac, F. Geniet, J. Leon, M. Taki, Nonlinear supratransmission in multicomponent systems, *Phys. Rev. Lett.* 105 (August) (2010) 074101.
[9] G. Kopidakis, S. Aubry, Discrete breathers and delocalization in nonlinear disordered systems, *Phys. Rev. Lett.* 84 (April) (2000) 3236–3239.
[10] G. Kopidakis, S. Aubry, Intraband discrete breathers in disordered nonlinear systems. II. Localization, *Physica D: Nonlinear Phenom.* 139 (May) (2000) 247–275.
[11] P. Maniadis, G. Kopidakis, S. Aubry, Energy dissipation threshold and self-induced transparency in systems with discrete breathers, *Physica D: Nonlinear Phenom.* 216 (March) (2006) 121–135.
[12] B. Yousefzadeh, A.S. Phani, Energy transmission in finite dissipative nonlinear periodic structures from excitation within a stop band, *J. Sound Vib.* 354

(June) (2015) 180–195.

[13] G. Yu, X. Wang, Z. Tao, Resonant emission of solitons from impurity-induced localized waves in nonlinear lattices, *Phys. Rev. E* 83 (February) (2011) 026605.

[14] A.B. Togueu Motcheyo, C. Tchawoua, J.D. Tchinang Tchameu, Supratransmission induced by waves collisions in a discrete electrical lattice, *Phys. Rev. E* 88 (October) (2013) 040901.

[15] B.P. Bernard, B.P. Mann, Passive band-gap reconfiguration born from bifurcation asymmetry, *Phys. Rev. E* 88 (November) (2013) 052903.

[16] B.P. Bernard, M.J. Mazzoleni, N. Garraud, D.P. Arnold, B.P. Mann, Experimental investigation of bifurcation induced bandgap reconfiguration, *J. Appl. Phys.* 116 (August) (2014) 084904.

[17] R. Khomeriki, S. Lepri, S. Ruffo, Nonlinear supratransmission and bistability in the Fermi–Pasta–Ulam model, *Phys. Rev. E* 70 (December) (2004) 066626.

[18] W. Atkinson, N. Cabrera, Motion of a Frenkel–Kontorowa dislocation in a one-dimensional crystal, *Phys. Rev.* 138 (May) (1965) A763–A766.

[19] J. Pouget, G.A. Maugin, Solitons and electroacoustic interactions in ferroelectric crystals. I. Single solitons and domain walls, *Phys. Rev. B* 30 (November) (1984) 5306–5325.

[20] J. Pouget, G.A. Maugin, Solitons and electroacoustic interactions in ferroelectric crystals. II. Interactions of solitons and radiations, *Phys. Rev. B* 31 (April) (1985) 4633–4649.

[21] F. Prengel, A. Wacker, E. Schöll, Simple model for multistability and domain formation in semiconductor superlattices, *Phys. Rev. B* 50 (July) (1994) 1705–1712.

[22] M. Brambilla, L.A. Lugiato, V. Penna, F. Prati, C. Tamm, C.O. Weiss, Transverse laser patterns. II. Variational principle for pattern selection, spatial multistability, and laser hydrodynamics, *Phys. Rev. A* 43 (May) (1991) 5114–5120.

[23] P. Marmillot, M. Kaufman, J. Hervagault, Multiple steady states and dissipative structures in a circular and linear array of three cells: *numerical and experimental approaches*, *J. Chem. Phys.* 95 (1991) 1206–1214.

[24] K.L.C. Hunt, J. Kottalam, M.D. Hatlee, J. Ross, Multiple steady states in coupled flow tank reactors, *J. Chem. Phys.* 96 (May) (1992) 7019–7033.

[25] J.P. Laplante, T. Erneux, Propagation failure and multiple steady states in an array of diffusion coupled flow reactors, *Physica A: Stat. Mech. Appl.* 188 (September) (1992) 89–98.

[26] J. Foss, A. Longtin, B. Mensour, J. Milton, Multistability and delayed recurrent loops, *Phys. Rev. Lett.* 76 (January) (1996) 708–711.

[27] R.S. Lakes, T. Lee, A. Bersie, Y.C. Wang, Extreme damping in composite materials with negative-stiffness inclusions, *Nature* 410 (March) (2001) 565–567.

[28] D.M. Kochmann, Stable extreme damping in viscoelastic two-phase composites with non-positive-definite phases close to the loss of stability, *Mech. Res. Commun.* 58 (June) (2014) 36–45.

[29] C.S. Wojnar, D.M. Kochmann, A negative-stiffness phase in elastic composites can produce stable extreme effective dynamic but not static stiffness, *Philos. Mag.* 94 (February) (2014) 532–555.

[30] R.L. Harne, M.E. Schoemaker, B.E. Dussault, K.W. Wang, Wave heave energy conversion using modular multistability, *Appl. Energy* 130 (June) (2014) 148–156.

[31] D. Restrepo, N.D. Mankame, P.D. Zavattieri, Phase transforming cellular materials, *Extreme Mech. Lett.* 4 (September) (2015) 52–60.

[32] N. Nadkarni, C. Daraio, D.M. Kochmann, Dynamics of periodic mechanical structures containing bistable elastic elements: *from elastic to solitary wave propagation*, *Phys. Rev. E* 90 (August) (2014) 023204.

[33] Z. Liu, X. Zhang, Y. Mao, Y.Y. Zhu, Z. Yang, C.T. Chan, P. Sheng, Locally resonant sonic materials, *Science* 289 (September) (2000) 1734–1736.

[34] Z. Liu, C.T. Chan, P. Sheng, Three-component elastic wave band-gap material, *Phys. Rev. B* 65 (April) (2002) 165116.

[35] N.X. Fang, D. Xi, J. Xu, M. Ambati, W. Srituravanich, C. Sun, X. Zhang, Ultrasonic metamaterials with negative modulus, *Nat. Mater.* 5 (June) (2006) 452–456.

[36] J. Li, C.T. Chan, Double-negative acoustic metamaterial, *Phys. Rev. E* 70 (November) (2004) 055602.

[37] Y. Ding, Z. Liu, C. Qiu, J. Shi, Metamaterial with simultaneously negative bulk modulus and mass density, *Phys. Rev. Lett.* 99 (August) (2007) 093904.

[38] Y. Lai, Y. Wu, P. Sheng, Z.-Q. Zhang, Hybrid elastic solids, *Nat. Mater.* 10 (June) (2011) 620–624.

[39] X.N. Liu, G.K. Hu, G.L. Huang, C.T. Sun, An elastic metamaterial with simultaneously negative mass density and bulk modulus, *Appl. Phys. Lett.* 98 (June) (2011) 251907.

[40] J.E. Macías-Díaz, A. Puri, An application of nonlinear supratransmission to the propagation of binary signals in weakly damped, mechanical systems of coupled oscillators, *Phys. Lett. A* 366 (April) (2007) 447–450.

[41] F. Farzbod, M.J. Leamy, Analysis of Bloch's method in structures with energy dissipation, *J. Vib. Acoust.* 133 (September) (2011) 051010.

[42] L.-f. Lou, *Introduction to Phonons and Electrons*, World Scientific Publishing Co., River Edge, New Jersey, 2003.

[43] G. Noh, K.-J. Bathe, An explicit time integration scheme for the analysis of wave propagations, *Comput. Struct.* 129 (August) (2013) 178–193.

[44] A.M. Balk, A.V. Cherkaev, L.I. Slepyan, Dynamics of chains with non-monotone stress–strain relations. II. Nonlinear waves and waves of phase transition, *J. Mech. Phys. Solids* 49 (January) (2001) 149–171.

[45] J.R. Raney, N. Nadkarni, C. Daraio, D. M. Kochmann, J.A. Lewis, K. Bertoldi. Stable propagation of mechanical signals in soft media using stored elastic energy, *Proc. Natl. Acad. Sci.* 113 (2016), 9722-9727.